Adsorption (2009) 15: 31–41
DOI 10.1007/s10450-008-9147-4

Interpretation of integrated gas sorption and mercury porosimetry studies of adsorption in disordered networks using mean-field DFT

Sean P. Rigby · Peter I. Chigada

Received: 23 January 2008 / Revised: 23 October 2008 / Accepted: 16 December 2008 / Published online: 8 January 2009

Abstract The presence of co-operative adsorption behaviour, operating between neighbouring pores within a disordered, void-space network, such as advanced adsorption effects, can significantly complicate the interpretation of gas adsorption data for complex porous solids, such as coked heterogeneous catalysts. The novel integrated gas sorption and mercury porosimetry method can be used to abstract the specific adsorption and desorption behaviour for particular, small sub-sets of similarly-sized pores contained within the complex network of a disordered porous solid. It will be shown in this work how, for ink-bottle geometries, the integrated experiments also allow the deconvolution of the gas sorption behaviour in pore necks, as well as pore bodies, and therefore enable the mechanism of desorption from the pore bodies to be determined. However, proper interpretation of the adsorption data from integrated experiments can be problematic using classical adsorption theories. In this work, it has been demonstrated that the experimental observations can be better understood in the light of mean-field DFT simulations of adsorption in representative pore models. Hence, a better description of the particular physical mechanisms underlying adsorption isotherms in disordered porous solids has been obtained. In addition, the new method allows more detail of the void space geometry to be obtained, such as the ratio of pore neck length relative to pore body length.

Keywords Adsorption · MFDFT · Mercury porosimetry · Hysteresis

S.P. Rigby (✉) · P.I. Chigada
Department of Chemical Engineering, University of Bath, Claverton Down, Bath, BA2 7AY, UK
e-mail: S.P.Rigby@bath.ac.uk

1 Introduction

Gas adsorption is a widely used technique to determine the pore size distributions (PSDs) of mesoporous media. The accuracy of the PSDs thereby obtained is often critical for correctly understanding the performance of one particular heterogeneous catalyst relative to another. The gas adsorption method is based upon the theory that the pressure at which capillary condensation of nitrogen occurs is a unique function of pore size. This pressure is given, for larger pores, by the Kelvin equation (Gregg and Sing 1982). However, for mesoporous solids, a hysteresis phenomenon is frequently observed for the isotherm; the pressure at which nitrogen evaporates from the sample on the desorption branch of the isotherm is generally lower than the pressure at which it originally condensed at on the adsorption branch. Hence, a long-standing research question has concerned determining which particular isotherm branch, and which corresponding theory or model equation, to use for calculating pore size distributions. Early work by Cohan (1938) suggested that the hysteresis arose from the different shapes of the respective menisci for adsorption and desorption. Cohan (1938) suggested that, for adsorption in an infinitely-long, cylindrical pore open at both ends, condensation occurred with a cylindrical meniscus, whilst, on desorption, the meniscus was hemispherical. The qualitative predictions of the Cohan model have recently been confirmed by both mean field (density functional) theory (MFT) and grand canonical Monte-Carlo (GCMC) simulations (Libby and Monson 2004). However, subsequent to Cohan's work, it was found that the shape of the desorption isotherm for disordered mesoporous solids is heavily influenced by network and percolation effects, such as pore-blocking (Gregg and Sing 1982). Hence, it was subsequently suggested that the adsorption branch should be used for calculating pore size distrib-

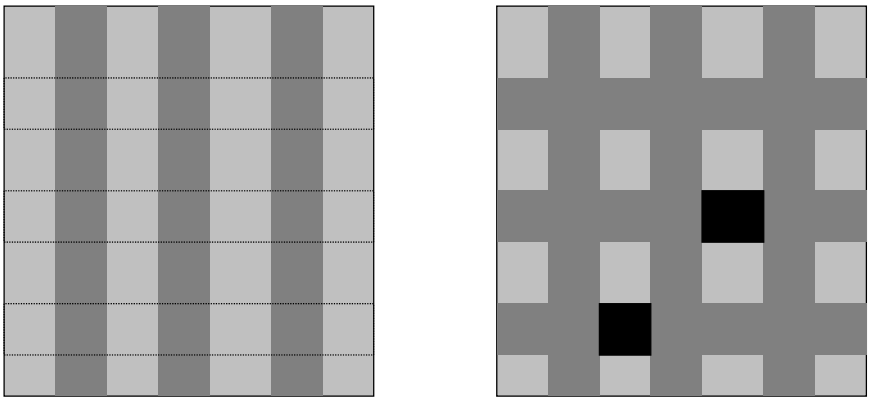

(a) (b)

Fig. 1 Schematic diagram depicting contrasting approaches to constructing model materials to study gas adsorption. **a** Start with simple elements (e.g. isolated, straight, cylindrical pores (*dark grey*) in MCM-41), and then add further complexity (*dashed lines* indicate potential addition of interconnections), *or* **b** start with a complex, inter-connected network (*dark grey*) and then remove simple elements (shown in *black*)

utions. In addition, the Barrett-Joyner-Halenda (BJH) algorithm (Barrett et al. 1951), and more sophisticated methods of determining PSDs, such as non-local density-functional theory (NLDFT) (Neimark and Ravikovitch 2001), assume that, within an interconnected network, the adsorption in each individual void space region defined as a pore occurs independently of surrounding pores. In order to test what is the appropriate technique to determine the PSD for a given material from gas sorption, it is necessary to utilize model materials for which an independent measure of the PSD is possible.

Conventionally experimental tests of adsorption theories (Morishige and Nakamura 2004), have utilized porous solids with purported simple and uniform pore structures, such as MCM-41, as model materials because they are designed to possess regular arrays of parallel, isolated, uniform cylindrical pores. Studies of adsorption in slightly more complex geometries are achieved by adding pore interconnections, such as with SBA-16, MCM-48 or KIT-5 (Morishige and Tateishi 2003; Morishige and Tarui 2007). However, recently (Rigby and Fletcher 2004; Rigby et al. 2008) a novel method to test adsorption theories, including the notion of independent pores, even in disordered, inter-connected pore network systems, has been proposed. This alternative approach involves taking a (potentially) much more complex, inter-connected pore network and removing simple elements, such as pores of a particular characteristic dimension. The two contrasting methods are shown schematically in Fig. 1. The new approach has been implemented using the novel integrated gas sorption and mercury porosimetry method (Rigby et al. 2008). This technique consists of a sequence of alternating gas sorption and mercury porosimetry experiments conducted in series on the same sample. This method is particularly powerful when applied to model systems with special characteristics.

Data from mercury porosimetry (Rigby et al. 2008) and magnetic resonance imaging (Hollewand and Gladden 1995) have demonstrated that a ∼3 mm diameter, mesoporous, sol-gel silica sphere, denoted S1 possesses macroscopic (∼100 μm) heterogeneities in the spatial distribution of pore size, such that the distribution is a macroscopic analogue of an 'ink-bottle' pore geometry. Spatially extensive, but isolated, regions of similarly-sized, larger pores are shielded by smaller pores. Since, the heterogeneities were macroscopic the 'neck' can be removed from the 'bottle' by fragmentation of the S1 pellets. In previous studies (Rigby et al. 2008) of this disordered system, using integrated gas sorption and porosimetry, it was shown (independently of gas sorption) that mercury becomes entrapped within S1, only in those pores with a very narrow range of radii, centered around 7.32 nm. In the integrated experiments, the subtraction of the nitrogen isotherms obtained following mercury entrapment, from the corresponding isotherms obtained beforehand, allowed deconvolution of the changes to the capillary condensation and evaporation processes occurring because of the presence, or lack thereof, of the sub-set of pores that entrap mercury. The shapes of the lowermost part of the hysteresis loop, and also the uppermost part, around the desorption knee, were identical before and after porosimetry, thus indicating that the presence of mercury did not influence capillary condensation in the pores filling, or emptying, in these parts of the isotherms. This may be due to the shielding effects of the surface multi-layer covering any boundary with entrapped mercury.

The key finding from these previous studies (Rigby et al. 2008) was that the relative pressure for capillary condensation, in the abstracted pores, was well predicted by the Cohan (1938) equation for a cylindrical meniscus, once the correct t-layer correction, appropriate to the particular degree of geometric and chemical heterogeneity of the surface of S1, had been made. Previous work (Rigby 2007) had suggested that the surface of sol-gel silicas is both chemically and geometrically heterogeneous. The above finding, from integrated experiments, appeared to suggest that the thermo-

dynamically independent pore model may still be valid for pores within certain relatively disordered networks.

One example of a key use of gas adsorption for characterizing disordered media, that absolutely requires an accurate knowledge of the underlying physical process such that the correct theory can be selected to analyse the raw data, is to follow the structural evolution of a mesoporous, heterogeneous catalyst during deactivation by coke deposition. In particular, whether, or not, the process known as 'advanced condensation' (Esparza et al. 2004) is occurring will significantly affect the interpretation required for the adsorption data, and thus the pore size distribution obtained, and ultimately the conclusions reached about the deactivation process. The advanced condensation theory (Esparza et al. 2004) is similar to proposals put forward by de Boer (1958). It proposed that, for a through (open) ink-bottle pore geometry, if the radius of the two shielding pore necks is greater than half that of the intermediate pore body then all will fill at the same pressure. In this case, the pressure required is equivalent to that given by the Cohan (1938) equation for a cylindrical meniscus in the pore neck. This is because once condensate has filled the pore neck, filling of the pore body may then proceed via ingress of the, now hemispherical, meniscus from the end of the pore neck. If the pore neck radius is over half that of the pore body, then the pressure for condensation within the pore body, for a hemispherical meniscus, is exceeded by the pressure required to condense in the neck with a cylindrical meniscus. Therefore, if an ink-bottle pore geometry is generated by progressive pore mouth blocking by coke deposition, then, in the presence of advanced adsorption, the pattern of adsorption (and hence data analysis necessary) would change as the neck radius declined below half that of the non-coked pore body. In addition, the strength of the adsorbate-catalyst and adsorbate-coke interactions may be different. Hence, to be able to properly study coking catalysts, it is essential to know if the advanced condensation effect is taking place, and which system parameters affect its occurrence. Advanced condensation theory is testable, as it makes a series of predictions. For example, if the neck of the ink-bottle could be removed, for example, by fragmentation of the sample, and advanced condensation was occurring beforehand, then a shift in the resulting composite adsorption isotherm to higher relative pressure should occur. This is because condensation in the de-shielded pore body would now occur at the higher pressure required for a cylindrical meniscus. For material S1 (Rigby et al. 2008), mercury intrusion data suggested that the shielding pore necks were ~90% of the size of the shielded pore body, and thus the pore body should have filled at the pressure required for a cylindrical meniscus in the pore neck. However, the finding that, instead, the Kelvin equation for a cylindrical meniscus in the pore body itself gave a good prediction of the condensation pressure in the pore body contradicts what would be expected from the advanced condensation theory. In addition, the shift in the adsorption isotherm on removing the pore shielding expected from advanced condensation theory was also not observed (Rigby et al. 2008).

Libby and Monson (2004) used MFT to study adsorption in open, ink-bottle pore geometries for slit-shaped, but not cylindrical, pores, and this work was solely in the abstract, with no direct comparison made to experimental findings. Libby and Monson (2004) also did not consider widely the effects, on adsorption, of the variation in the ratio of pore body size to pore neck size, and its potential interaction with the adsorbate-adsorbent interaction strength, to determine when these give rise to advanced condensation-type effects. The MFT method is particularly suitable for studying the effects of these interactions because both geometric and chemical heterogeneity can be readily incorporated into the model.

In this work, a novel data analysis approach will be described that demonstrates how results from the new integrated gas sorption and mercury porosimetry technique can be used to deconvolute the particular sorption behaviour of specific short pore necks, in addition to that for certain pore bodies as described in earlier work (Rigby et al. 2008). As described above, previous experimental results suggest that the classical advanced condensation theory does not appear to be correct for a sol-gel silica material. MFT will be used to understand why the classical theory does not work in this case by studying adsorption in a model of the real material. In addition, MFT has been used to validate a particular interpretation made of integrated gas sorption and mercury porosimetry data that demonstrated the importance of the influence of pore length on gas sorption. MFT will be used, in each case, to confirm that the specific effects suggested by the proposed particular interpretations of the experimental data are physically realizable, and then also explore the implications of these effects more generally.

2 Theory

2.1 Lattice-based, mean-field (density functional) theory (MF(DF)T)

In MFT (Libby and Monson 2004), for a single occupancy lattice gas with nearest neighbour interactions in an external field that determines the pore geometry, the grand potential, Ω, associated with the lattice gas Hamiltonian can be written as:

$$\Omega = kT \sum_i [\rho_i \ln \rho_i + (1-\rho_i)\ln(1-\rho_i)] + \sum_i \rho_i (\phi_i - \mu) - \varepsilon_{ff} \sum_{i<j} \rho_i \rho_j, \quad (1)$$

where ρ_i is the local density at site i, k is Boltzmann's constant, T is absolute temperature, μ is the chemical potential, ϕ_i denotes the external field at site i, and ε_{ff} is the strength of nearest neighbour interaction. $1/kT$ is denoted β. In this work ϕ_i is a field generated by treating the pore walls as made up of layers of atoms with a Lennard-Jones potential between these atoms and the sites of the lattice model:

$$\phi_i = 4\varepsilon_{mf}\left\lfloor(\sigma/r)^{12} - (\sigma/r)^6\right\rfloor, \tag{2}$$

where ε_{mf} described the energy of interaction (well-depth) and σ is the characteristic length-scale. The necessary condition for an equilibrium state (a minimum in Ω) is that the partial derivative of Ω with respect to local density at each site vanishes. Applying this condition to (1) and rearranging yields the following set of nonlinear algebraic equations that can be solved iteratively to yield the density distribution at a given value of μ and T:

$$\rho_i = \frac{1}{1 + \exp[(-\varepsilon_{ff}\sum_j \rho_j + \phi_i - \mu)/kT]}, \tag{3}$$

where the summation over j is taken over the nearest neighbours of site i.

Adsorption isotherms can be obtained by gradually incrementing the chemical potential, from a large negative value, in small steps to mimic the process in the real experiment. At the start, the adsorbate densities were set to a small value below that encountered in the isotherm to mimic the initial near-vacuum state in experiments, and subsequently each initial guess for the set of densities at each isotherm point was taken as the solution set for the last isotherm point. Desorption isotherms were obtained in a similar manner by decreasing the chemical potential for each step. Equilibrium isotherms were obtained in a different way, as described by Kierlik et al. (2002). At each value of chemical potential, the set of initial density configurations corresponding to uniform filling with densities in the range 0.01 to 1.0 were used as the starting points to determine the solution for the density distribution. For each value of initial uniform density, the grand potential for the final solution was determined. The final solution with the minimum grand potential was assigned as the equilibrium point. This search is not exhaustive of all potential initial configurations, particularly non-uniform configurations, but Kierlik et al. (2002) suggest this procedure gives rise to a good approximation to the equilibrium isotherm. The convergence criterion for the solution was such that the root mean square residual between succeeding solutions in the iterative scheme was below a particular tolerance level, typically $\sim 10^{-6}$. Since it is conceivable that the results may be sensitive to the particular metastable states identified, particularly for the simulations of adsorption and desorption, the sensitivity of the results to the iteration algorithm was tested. Two approaches were used. First, the algorithm used by Libby and Monson (2004) consisted of using only the values of ρ_i obtained in the 'previous round' of the iteration in (3) for the current round. Second, an alternative iterative process involved using the 'best guess' for ρ_i available at any point in time, and thus could involve a mixture of values from previous and present rounds of iteration for a given lattice site.

For a lattice gas model, the chemical potential at saturation is known analytically, and is given by $\mu_0 = -Z\varepsilon_{ff}/2$ (and thus for the simple cubic lattice used in this work, $\mu_0 = -3\varepsilon_{ff}$) (Libby and Monson 2004). The simulated isotherms obtained can thus be presented as density against relative activity, λ/λ_0, where $\lambda = \exp(\mu/kT)$, as well as against chemical potential. Apart from the potential effect of gas imperfection, this is equivalent to plotting the isotherms as a function of relative pressure, P/P_0, where P_0 is the saturation pressure.

2.2 Pore models

Two different pore models were studied in this work. The first model was a random cluster (RC) used to test the iterative scheme to solve equations of the form of (3), as used by Kierlik et al. (2002). The RC consisted of a cubic lattice within which the cubic lattice sites were occupied at random up to some specified fractional occupancy (Elias-Kohav et al. 1991). The second model was an ink-bottle pore system consisting of two cylindrical necks either side of a cylindrical pore body, as shown schematically in Fig. 2. The diameters and lengths of each pore segment could potentially be varied independently. The ink-bottle pore model also possessed two bulk reservoirs at the entrance to each pore neck. In all cases periodic boundary conditions were used for the lattice.

It is proposed that the second model includes the key characteristics of the material S1 that influence the form of the results from gas sorption and mercury porosimetry. Previous work (Rigby et al. 2008) using NMR cryoporometry has demonstrated that the pores of S1 are cylindrical. Analysis of mercury porosimetry data, for both whole and fragmented samples of pellets from batch S1, using novel semi-empirical alternatives to the Washburn equation (Rigby et al.

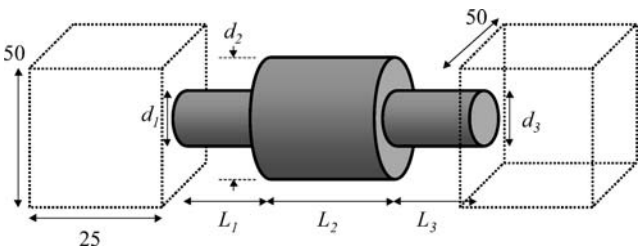

Fig. 2 Schematic diagram of model ink-bottle pore used in MFT simulations. Dimensions marked in lattice units. The volumes marked by dashed lines are the bulk reservoirs

2003), suggested that a macroscopically spatially-extensive region of larger pores was shielded by a skin of smaller pores at the pellet surface. As mentioned above, MRI studies (Hollewand and Gladden 1995) of pellets from batch S1 have shown that there are macroscopic heterogeneities in the spatial arrangement of pore size. The MRI results also suggest that the interpretation of a (neutron or X-ray) scattering curve in terms of one single correlation function would be flawed since the sample is not statistically uniform over length-scales in excess of the radiation wavelengths. Hence, scattering could not be used to construct a suitable void space model from a single correlation function, in this case. The observed high degree of spatial correlation of pore sizes in S1 suggests that a conventional random pore bond network model, where many different pore sizes are intermingled with each other, is also inappropriate in this case. Most interconnections between pores, at the pore scale, are between pores of similar size. Hence, a whole region of larger pores, shielded at the periphery by narrow necks, can be represented by the second model described above because the interconnections between pores of different sizes, apart from the necks, are not important in determining the shielding behaviour.

3 Experimental results

The material studied in this work is a commercially available, sol-gel silica sphere of diameter ∼2–3 mm, denoted S1, with a nitrogen BET monolayer capacity of 61.3 $cm^3(STP)g^{-1}$, a BET surface area of 267 $m^2\,g^{-1}$ (assuming a close packed monolayer, and standard cross-sectional area (Rouquerol et al. 1999)), and a specific pore volume of 1.02 $cm^3\,g^{-1}$. For a nitrogen BET fit over the range $0.05 < P/P_0 < 0.4$, the BET constant was 42.3.

Raw mercury porosimetry data for batch S1 obtained in earlier work (Rigby et al. 2008), and analysed using independently-calibrated, semi-empirical alternatives to the Washburn equation described previously (Rigby and Edler 2002), are shown in Fig. 3. From Fig. 3, it can be seen that the mercury retraction curve for a powdered sample of S1 completely overlays the corresponding powdered sample mercury intrusion curve when each are analysed using the appropriate alternatives to the Washburn equation (allowing for the experimental error present in the empirical equations). Hence, structural hysteresis and mercury entrapment have both been removed by fragmenting the sample. This finding suggests that pore 'shielding' effects have thus been removed by fragmentation, and consequently the mercury intrusion curve for the powdered sample represents the unshielded PSD for the material. It is likely that the macroscopic spatial correlation in the distribution of pore size, observed in the NMR images (Hollewand and Gladden 1995),

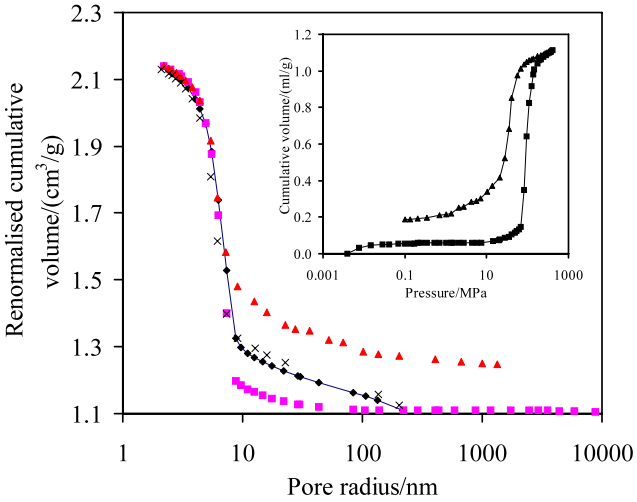

Fig. 3 Mercury porosimetry data for whole (■ intrusion, ▲ extrusion) and powdered (◆ intrusion, × extrusion) samples from batch S1 analysed using semi-empirical alternatives to the Washburn equation (Rigby and Edler 2002). The ultimate intrusion volume for the whole pellet sample has been renormalised to that for the powder sample to facilitate direct comparison of the intra-particle intrusion. The *inset* shows the raw data for the whole pellet sample

means that once a pellet is fragmented to particles with sizes of the order of the structural heterogeneities then shielding effects are removed (Rigby and Edler 2002).

For comparison purposes, Fig. 3 also shows mercury porosimetry data for a whole pellet sample from batch S1. This raw porosimetry data has also been analysed using the semi-empirical alternatives to the Washburn equation (Rigby and Edler 2002). In order to more easily compare the data-sets for whole and powdered samples, the ultimate intrusion volume for the whole pellet data has been renormalised to that obtained for the powder sample. From Fig. 3 it can be seen that the analysis of the raw porosimetry data for the whole pellet sample, using the alternatives to the Washburn equation, leads to a good overlap of the intrusion and extrusion curves at smaller pore radii. In addition, it is noted that the intrusion curve for the powdered sample also overlays the intrusion curve for the whole pellet sample at smaller pore radii. This similarity between intrusion curves for whole and powdered material was repeatable between different samples from the same batch, and thus suggests there is little intra-batch variability, as it must be smaller than the ∼4–5% error present in the alternatives to the Washburn equation due to their semi-empirical origin. Since the mercury intrusion curve for the powdered sample represents an unshielded PSD, the size of the pores containing the entrapped mercury can be obtained by subtracting the whole pellet mercury extrusion curve from the powder intrusion curve. For any range of the PSD within which entrapment occurs, the volume of mercury extruded will be less than that intruded, whereas this will not be the case for

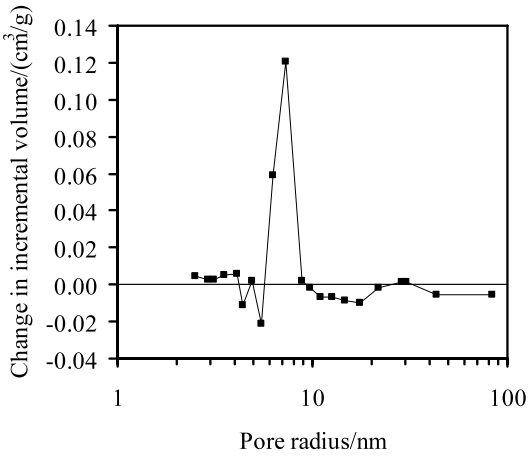

Fig. 4 Variation with pore radius of the difference in incremental volumes (using the same set of pore size bins) between the powder intrusion curve and whole pellet extrusion curve shown in Fig. 3

ranges where no entrapment occurs. Figure 4 shows the difference in incremental volumes over the same set of bins in pore size for the powder intrusion curve and the whole pellet extrusion curve. From Fig. 4 it can be seen that there is very little difference in the incremental volumes between the two curves except for a relatively narrow peak occurring at a radius of 7.32 ± 0.37 nm (where the quoted error arises from the empirical nature of the alternatives to the Washburn equation). As expected, the peak in Fig. 4 occurs at the pore radius where the powder intrusion and whole pellet extrusion cumulative curves diverge in Fig. 3.

The close similarity between the powder intrusion curve and the whole pellet extrusion curve for pore sizes either side of ~7.32 nm in Fig. 4 suggests that there is no residual structural hysteresis in these pore size ranges, and thus no delayed retraction, due to lack of mercury snap-off, during the initial stages of pressure reduction. A comparison of the mercury intrusion curves for whole and fragmented samples from batch S1 (shown in Fig. 3) suggests that the size of the pores shielding pores of radius 7.32 nm must be in the range 7.32–6.28 nm (mean ~6.8 nm), since the whole and powder intrusion curves overlay each other for pore sizes <6.28 nm. This suggests the abstracted pores are of shape group II, and, according to de Boer (1958), (advanced) adsorption should proceed in one step at the relative pressure corresponding to a cylindrical meniscus for the shielding pore radius.

From integrated nitrogen adsorption experiments, by subtracting the isotherms obtained after porosimetry from those obtained before (see Fig. 5), it was possible to deconvolute the sorption behaviour of the pores abstracted by the entrapment of mercury. The difference plots obtained previously (Rigby et al. 2008) for a typical sample from batch S1 are shown in Fig. 6. From Fig. 6, it can be deduced that adsorption in the pores of S1, within which mercury became entrapped, occurred predominantly at a relative pressure of

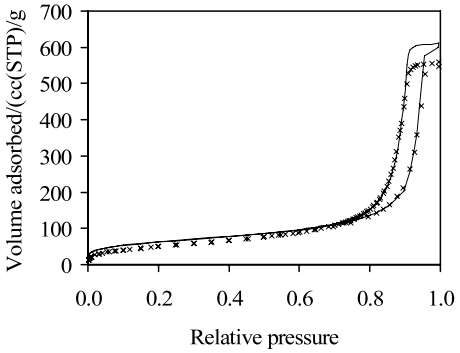

Fig. 5 Nitrogen sorption isotherms from before (*solid line*) and after (×) a mercury porosimetry experiment on a typical sample from batch S1

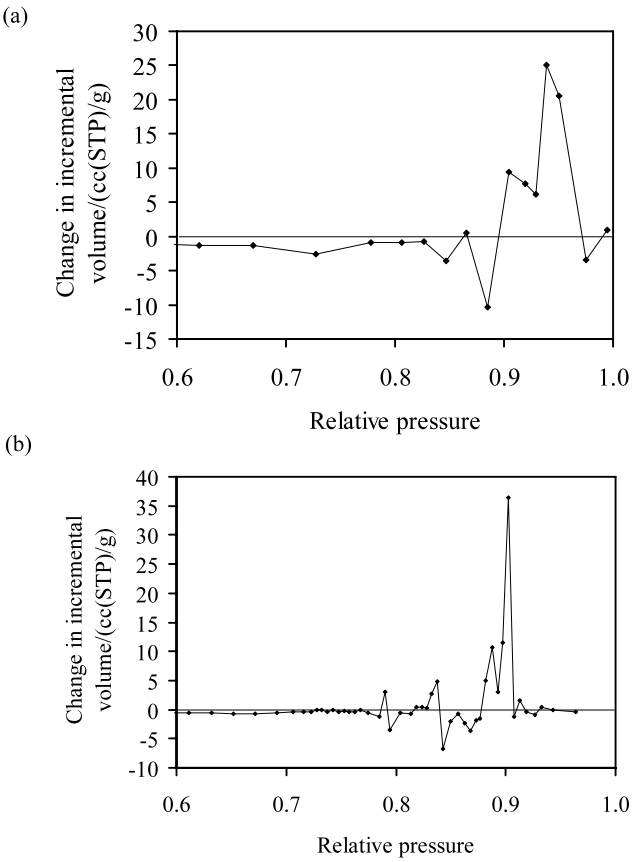

Fig. 6 Variation with relative pressure of the difference in incremental volumes between **a** adsorption and **b** desorption isotherms from before and after mercury entrapment in a sample from batch S1. The *lines* shown are to guide the eye

~0.939, while desorption from these pores occurred at a relative pressure of ~0.903. It was also found (Rigby et al. 2008) that there was no significant shift to higher relative pressure in the adsorption isotherm when pore shielding is removed following pellet fragmentation.

4 MFT simulations

Initially, the sensitivity of the simulation results to arbitrary (non-physical) aspects of the modelling procedure was tested. MFT simulations were conducted on random cluster models of disordered porous media generated on cubic lattices with side-lengths of 48 and 100 sites. The fraction of occupied lattice sites was 0.25. In these simulations the adsorbate-adsorbent interactions were modelled as a square well potential nearest-neighbour only interaction characterised by ε_{mf}, the strength of nearest neighbour adsorbate-adsorbent interaction. For the simulations the values of ε_{ff}, the strength of nearest neighbour adsorbate-adsorbate interaction, and ε_{mf}, the strength of nearest neighbour adsorbate-adsorbent interaction, were 5/3 and 2.5, respectively. The simulated isotherms, employing either the 'previous round' or 'best guess' iterative methods, for a RC model generated on a lattice with a side-length of 100 sites were obtained (not shown). It was found that the iteration algorithm used makes no difference to the shape of the isotherms, and this result was also replicated for the lattice side-length of 48 sites also used. In subsequent work reported here the 'previous round' iteration method of Libby and Monson (2004) was thus used.

Simulated adsorption isotherms were obtained for a number of open ink-bottle pore geometries, with cylindrical pore segments, for which the pore diameters, d_1–d_3, and pore lengths, L_1–L_3, respectively, were varied but not the interaction parameters. Simulations were also conducted on models with identical pore geometry but with varying Lennard-Jones parameters for the adsorbate-adsorbent interaction strength. For the simulated adsorption isotherms, in each case, the chemical potential (or activity) at the maximum in the rate of variation of density with chemical potential (*i.e.* the point at which the largest step increase in adsorbate density occurred) was obtained for both the pore and neck regions of the pore model, as defined in Fig. 2. These values are given in Table 1 for open ink-bottles. Examples of typical simulated isotherms are shown in Fig. 7.

By comparing the results shown in Fig. 8 for models with identical geometry but differing interaction parameters, both for strong and weak adsorbate-adsorbent interaction strength, in open ink-bottles, it can be seen that there is a transition from two-step to one-step overall adsorption, as the ratio of pore neck to pore body size, ξ $(= d_1/d_2$ or $d_3/d_2)$, approaches unity. However, the actual value of ξ, at which the transition from identical activities (for the largest steps in adsorption for within the pore body and within the pore necks) to different activities occurs, shifts to higher values for stronger adsorbate-adsorbent interactions, at fixed pore length. Hence, contrary to the classical theory of de Boer (1958) and others (Esparza et al. 2004) based on the Kelvin equation, the critical lower limit on ξ for advanced condensation is not fixed at 0.5 for cylindrical pore

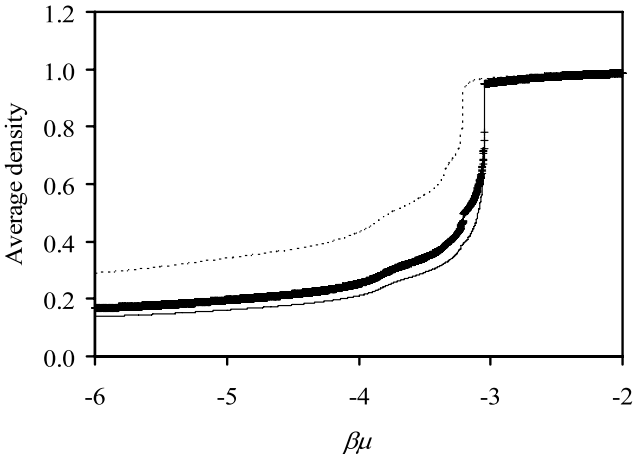

Fig. 7 Simulated adsorption isotherms for the pore necks (*dashed line*), the pore body (*solid line*), and overall composite pore (+), for an open ink-bottle pore model, as shown in Fig. 2 ($d_1 = d_3 = 14$; $d_2 = 40$; $L_1 = L_2 = L_3 = 44$; $\sigma = 0.89089$; $\beta\varepsilon_{mf} = 3$). The adsorbate density has been averaged over the relevant void space segment

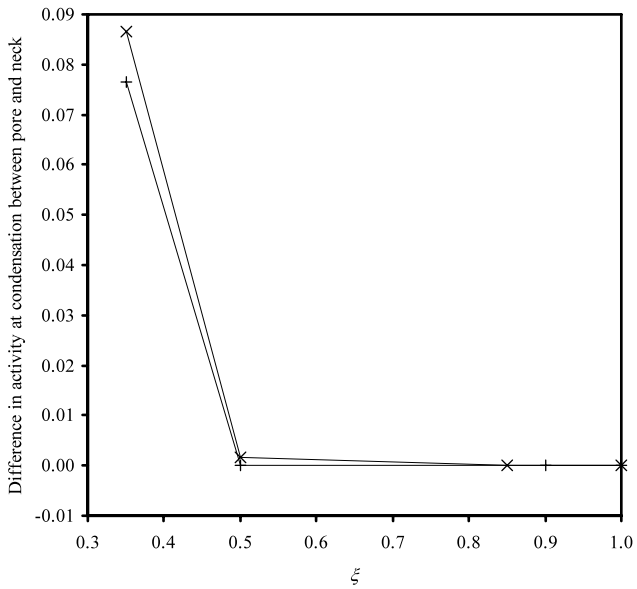

Fig. 8 Variation of the difference in the relative activity at condensation, between pore body and pore neck, as a function of pore neck to pore body size ratio (ξ) for both strong ($\sigma = 0.89089$; $\beta\varepsilon_{mf} = 3$; $d_2 = 40$; $L_1 = L_3 = 10$, $L_2 = 44$) (×, *solid line*) and weak ($\sigma = 1$, $\beta\varepsilon_{mf} = 1.25$; $d_2 = 40$; $L_1 = L_3 = 10$, $L_2 = 44$) (+, *dashed line*) adsorbate-adsorbent interaction strength

geometry, but varies according to the strength of adsorbate-adsorbent interactions. It can also be seen from Fig. 9, that a comparison of the results for models with identical interaction parameters, and the same pore lengths and ratios of neck diameter to body diameter, but different absolute body diameters, shows that the value of ξ, at which the transition occurs, also increases with decreased pore body size. A fully wetting fluid (e.g. as nitrogen is assumed to be in the

Table 1 Results of MFT simulations of gas adsorption in model ink-bottle pores. Parameters are as defined in Fig. 2 and in the text

σ	$\beta\varepsilon_{mf}$	d_1 and d_3	L_1 and L_3	d_2	L_2	ξ	$\beta\mu$ at neck condensation	$\beta\mu$ at pore condensation	λ/λ_0 at neck condensation	λ/λ_0 at pore condensation
1	1.25	14	10	40	44	0.35	−3.12667	−3.04333	0.8810	0.9576
1	1.25	20	10	40	44	0.5	−3.04333	−3.04333	0.9576	0.9576
1	1.25	36	10	40	44	0.9	−3.02167	−3.02167	0.9786	0.9786
1	1.25	40	10	40	44	1	−3.02	−3.02	0.9802	0.9802
0.89089	3	–	–	36	44	–	–	−3.02333	–	0.9769
0.89089	3	–	–	40	44	–	–	−3.01667	–	0.9835
0.89089	3	14	10	40	44	0.35	−3.14	−3.045	0.8694	0.9560
0.89089	3	20	10	40	44	0.5	−3.04667	−3.045	0.9544	0.9560
0.89089	3	34	10	40	44	0.85	−3.02333	−3.02333	0.9769	0.9769
0.89089	3	36	10	36	44	1	−3.02667	−3.02667	0.9737	0.9737
0.89089	3	36	10	40	44	0.9	−3.02167	−3.02167	0.9786	0.9786
0.89089	3	40	10	40	44	1	−3.02167	−3.02167	0.9786	0.9786
0.89089	3	14	44	40	44	0.35	−3.205	−3.045	0.8146	0.9560
0.89089	3	20	44	40	44	0.5	−3.09	−3.045	0.9139	0.9560
0.89089	3	24	44	40	44	0.6	−3.06333	−3.045	0.9386	0.9560
0.89089	3	28	44	40	44	0.7	−3.04667	−3.04333	0.9544	0.9576
0.89089	3	34	44	40	44	0.85	−3.04	−3.04	0.9608	0.9608
0.89089	3	36	44	36	44	1	−3.03167	−3.03167	0.9688	0.9688
0.89089	3	36	44	40	44	0.9	−3.03	−3.03	0.9704	0.9704
0.89089	3	40	44	40	44	1	−3.025	−3.025	0.9753	0.9753
0.89089	3	16	44	20	44	0.8	−3.14833	−3.125	0.8621	0.8825
0.89089	3	17	44	20	44	0.85	−3.12833	−3.125	0.8796	0.8825
0.89089	3	18	44	20	44	0.9	−3.115	−3.115	0.8914	0.8914
0.89089	3	20	44	20	44	1	−3.09167	−3.09167	0.9124	0.9124
0.89089	3	9	44	10	44	0.9	−3.48667	−3.45833	0.6147	0.6323
0.89089	3	36	10	36	88	1	−3.03	−3.03	0.9704	0.9704
0.89089	3	36	10	40	88	0.9	−3.025	−3.025	0.9753	0.9753
0.89089	3	40	10	40	88	1	−3.025	−3.025	0.9753	0.9753
0.89089	3	36	10	0	–	–	−3.045	–	0.9560	–
0.89089	3	36	44	0	–	–	−3.05	–	0.9512	–
0.89089	3	36	88	0	–	–	−3.04667	–	0.9544	–
0.89089	3	40	88	0	–	–	−3.04167	–	0.9592	–

Notes: $\beta\varepsilon_{ff} = 1.0$ in all cases; $\Delta(\beta\mu) = (5/3) \times 10^{-3}$ in all cases

Kelvin equation) would presumably correspond to the case of strong adsorbate-adsorbent interactions but the results obtained here show that independent adsorption can occur in pore bodies for values of ξ above 0.5.

The results in Fig. 10 (and Table 1) show that, for relatively short, uniform pores (*i.e.* identical neck and body sizes), at fixed strength of adsorbate-adsorbent interactions, the activity at which adsorbate condenses decreases with increased pore length, as might be expected, since a longer pore must represent a deeper potential well. However, as pores become longer still, the condensation step activity becomes independent of pore length. In addition, the length of a pore neck also alters the advanced condensation behaviour. For short necks the critical value of ξ is about 0.5, but for longer necks the critical value of ξ is higher.

For simulated adsorption, from Table 1, it can be seen that, at a high strength of adsorbate-adsorbent interactions ($\beta\varepsilon_{mf} = 3$), for ink-bottle pores with short necks ($L_1 = L_3 = 10$) and with $\xi \geq 0.9$ ($d_1 = d_3 = 36$; $d_2 = 40$), capillary condensation occurs in a single step at the activity corresponding to that for condensation in a uniform pore of equivalent total length, and diameter equal to that of the *body* of the ink-bottle pore ($d_1 = d_2 = d_3 = 40$). This effect is independent of the length of the pore body, over the range of

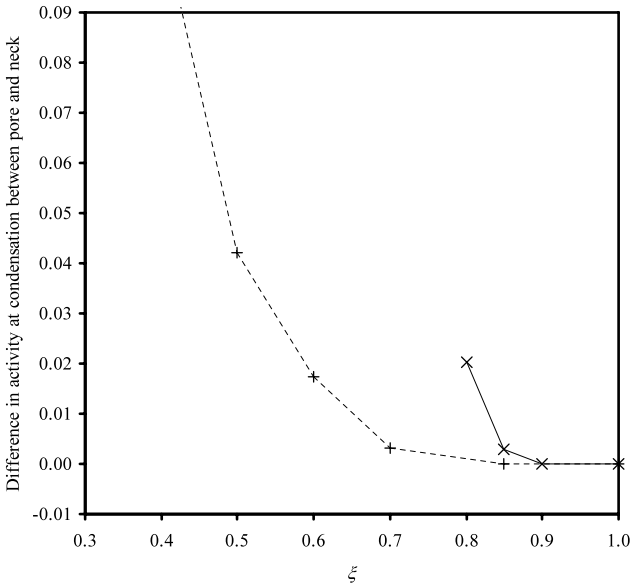

Fig. 9 Variation of the difference in the relative activity at condensation, between pore body and pore neck, as a function of pore neck to pore body size ratio (ξ) for strong adsorbate-adsorbent interaction strength and long necks ($\sigma = 0.89089$; $\beta\varepsilon_{mf} = 3$; $L_1 = L_3 = 44$, $L_2 = 44$) but different absolute pore body size ($d_2 = 20$, $\times$ and *solid line*; $d_2 = 40$, $+$ and *dashed line*)

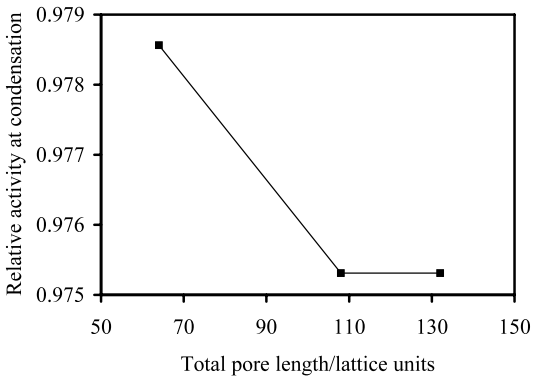

Fig. 10 Variation of relative activity at condensation with total pore length ($\sigma = 0.89089$; $\beta\varepsilon_{mf} = 3$; $d_1 = d_3 = d_2 = 20$)

lengths studied ($L_2 = 44$–88). In addition to the adsorption isotherms, for the ink-bottle pores with short necks and with $\xi \geq 0.9$, the equilibrium isotherms were also determined using the algorithm proposed by Kierlik et al. (2002) described above. It was found that the main condensation transition in the overall adsorption isotherm corresponded to that for the overall equilibrium isotherm in these cases. For ink-bottle pores with short necks, and where ξ is large but $\xi < 0.9$, capillary condensation is also single-step but occurs at activities less than that required for condensation in a uniform pore of equivalent total length, and of a diameter equal to that of the body of the ink-bottle pore.

5 Discussion

The results obtained above suggest that, rather than the two behavioural regimes envisaged by advanced condensation theory based on the Kelvin equation, the condensation process in open ink-bottle pores falls into three behavioural regimes. For larger values of ξ, condensation in the pore body and neck occur at the same relative activity, but not that required for an open, uniform, cylindrical pore of the same length and diameter as the pore neck. At low values of ξ condensation is a two-step process, and occurs in the pore body at a relative activity that is the square of the relative activity for condensation in an open, uniform, cylindrical pore of the same length and diameter. This behaviour is equivalent to pore body filling from a hemispherical meniscus originating at the boundary with the pore neck, as predicted by the Kelvin equation. However, between these two regimes, there is also a transitional regime where condensation in the ink-bottle pore is a two-step process but the relative activity for condensation in the pore body is higher than that required from a hemispherical meniscus.

For the material S1 described above, mercury porosimetry indicates that $\xi \approx 0.9$ for the ink-bottle pores in which mercury becomes entrapped within the pore bodies during an integrated gas sorption and mercury porosimetry experiment. The integrated gas adsorption experiments also indicated that condensation in these pore bodies occurred at the relative activity expected for a long, uniformly cylindrical pore of the same diameter as the pore body. Hence, these experimental findings are in line with the simulations for the ink-bottle pores with short necks and $\xi \geq 0.9$. It is also noted that the experimental studies (Rigby et al. 2008) indicated that the surfaces of the particular pore bodies, in which mercury became entrapped, were characterised by a BET constant of 439 for nitrogen, which is considered (Rouquerol et al. 1999) a very high value for nitrogen that is characteristic of strong adsorbate-adsorbent interactions.

Whilst not described previously (Rigby et al. 2008), it is also the case that, for ink-bottle-type geometries, integrated gas sorption and mercury porosimetry experiments additionally allow the deconvolution of the gas sorption behaviour in the pore necks, as well as the pore bodies, and thereby permit a determination of the mechanism of desorption from the pore bodies. The stages of the process by which this may be achieved are shown schematically in Fig. 11, and are explained as follows. As deduced above, for ink-bottle pores with short necks and $\xi \geq 0.9$, such as those found in S1, adsorption in the entire open, ink-bottle pore occurs as a single step, as shown in stage (i) in Fig. 11. However, at stage (ii), once mercury becomes entrapped within, and completely fills, the pore body, this turns the pore necks into short dead-end pores. Since adsorption can then commence from a hemispherical meniscus, with the same diameter as

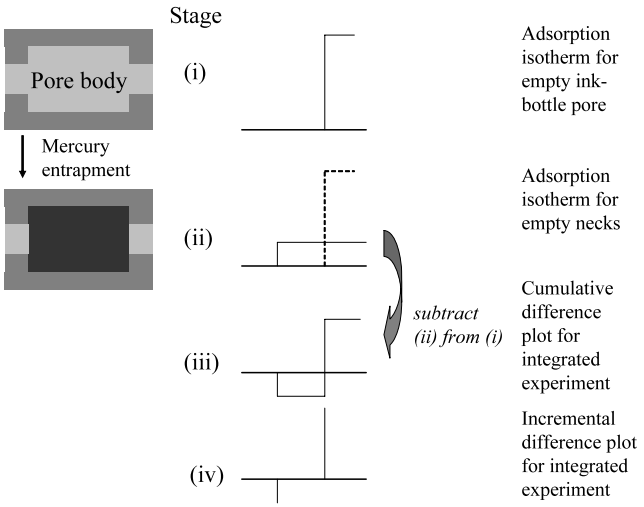

Fig. 11 Schematic diagram depicting proposed scenario leading to incremental difference plot for adsorption isotherms from integrated porosimetry experiment for S1 shown in Fig. 6

the pore neck, in the new dead-end pores, then this is likely to shift the relative activity at which adsorption occurs in the necks to a new lower value, as shown in stage (ii) in Fig. 11. The overall total pore volume has been reduced, and thus the amount adsorbed is also reduced. At stage (iii), the adsorption isotherm obtained for the sample following porosimetry (at stage (ii)) is subtracted from the isotherm for the fresh sample (stage (i)) to generate a cumulative difference plot for the two isotherms. Finally, at stage (iv), this cumulative plot is converted to an incremental difference plot. The isotherm subtraction process means a negative peak in the difference plot will occur at the relative activity at which the pore necks fill from a hemispherical meniscus, since no adsorption occurred there for the fresh sample. In the incremental difference plot, for the adsorption isotherms for batch S1, shown in Fig. 5, a negative peak occurs at a relative pressure of 0.885, which is lower than that for the main positive peak of 0.939 corresponding to where adsorption occurred at stage (i).

If desorption from the pore body of an open, ink-bottle pore is controlled by pore-blocking effects due to the adjacent necks, then the relative activity at which desorption occurs from the pore body should be the same as that for the pore neck. As stated above, MFT simulations conducted by Libby and Monson (2004) have confirmed the classical theory of Cohan (1938) that no hysteresis should occur between adsorption to, and desorption from, dead-end pores, as both originate via hemispherical menisci. The simulations described (Libby and Monson 2004) also showed that desorption from open ended pores occurred at the same relative activity as desorption from dead-end pores of the same diameter. Hence, the relative pressure for desorption from pore bodies should be equal to that for both adsorption and desorption, via a hemispherical meniscus, for the pore neck. In the difference plot for the desorption isotherms obtained before and after porosimetry for a sample from batch S1 shown in Fig. 6b, the main positive peak corresponds to (at least) the desorption from the pore bodies. If desorption from the pore bodies in fresh samples of S1 (that go on to get abstracted during the course of integrated porosimetry experiments) is controlled by pore blocking, then the relative pressure for the main positive peak in the difference plot for desorption (Fig. 6b), should correspond with the negative peak in the difference plot for adsorption (Fig. 6a), since the latter is for adsorption (or desorption as adsorption is reversible in dead end pores) via a hemispherical meniscus from the pore necks. Given the finite nature of the pressure steps in the adsorption difference plot the main negative peak corresponds to the range of relative pressures of ∼0.865–0.905, which straddles the peak value of the main peak (0.9026) in the desorption difference plot. The findings from the integrated experiment are thus consistent with pore blocking controlling the desorption of condensed phase from the pore bodies abstracted by the porosimetry experiment.

The simulations described above suggest that the experimental observation, that condensation in the initially shielded (and subsequently abstracted) pore bodies occurs at the relative activity required for a cylindrical meniscus in the pore body, implies that the shielding pore necks are short compared to the pore body length. Two further sets of findings suggest that the necks guarding the abstracted pore bodies in S1 are relatively short. The total length of pores of a given size is proportional to V_i/r_i^2, where V_i is the incremental specific pore volume of pores in bin i of radius r_i. From a consideration of the relative total specific pore volumes constituting the main positive peak (relative pressures ∼0.9045–0.975) and the main negative peak (relative pressures of ∼0.865–0.905) in the adsorption difference plot, and assuming that the likely pore neck radius was ∼6.8 nm, as shown by porosimetry, then the average ratio of the pore body length to neck length is ∼6. This result is in line with the simulations, which suggested that adsorption in open, ink-bottle pores was single step when $\xi \sim 0.9$ for ratios of pore body length to neck length ≥4.4. In previous work (Rigby et al. 2008), it was found that the experimental relative pressure for desorption from the abstracted pore bodies was higher than that predicted from the Kelvin equation for desorption via a hemispherical meniscus with a radius of curvature relevant to the pore body size. The results of the simulations described above suggest that relatively short pores have higher relative activities for phase transitions than longer pores with the same diameter. Hence, it seems likely that the elevated relative pressure for desorption from the pore necks in S1 may be due to their short length. It is noted that it has been suggested previously, based upon analysis of mercury porosimetry data

alone (Rigby et al. 2003), that larger pore bodies within pellets of S1 are shielded by a narrow band of pore necks at the pellet surface.

6 Conclusions

MFT simulations have shown that the scenario envisaged, by advanced adsorption theory (AAT), for capillary condensation in open, ink-bottle pores is too simplistic. MFT simulations suggest that, instead of the two size regimes suggested by AAT, there are three regimes of behaviour depending on the ratio of pore neck size to pore body size (ξ). The MFT simulations have confirmed the observation, from integrated gas sorption and mercury porosimetry experiments, that adsorption in an open, ink-bottle pore with $\xi \geq 0.9$ occurs at a relative activity corresponding to that for a cylindrical meniscus in the pore body, if the neck is short. It has been demonstrated that integrated adsorption and porosimetry experiments can also deconvolve the separate adsorption and desorption behaviour within pore necks, in addition to that for pore bodies becoming filled with entrapped mercury, and thereby demonstrate the mechanism of desorption from a particular sub-set of pores in a material. This has also enabled the estimation of the typical ratio of pore body to pore neck length for a particular sub-set of ink-bottle pores within S1. This result, together with additional findings, suggest that the apparently, anomalously high relative activity for desorption from the abstracted pores in S1 is due to the short length of the shielding necks. The above findings suggest that great care must be taken when interpreting any apparent temporal evolution in pore size distributions obtained from nitrogen adsorption data for a series of progressively coked catalyst samples.

Nomenclature

d pore model section diameter
k Boltzmann constant (1.380662×10^{-23} JK^{-1})
L pore model section length
r distance, lattice units
r_i pore radius in bin i, m
T absolute temperature, K
V_i specific incremental volume of pores in bin i, m^3 g^{-1}

Greek letters

β $1/kT$
ε_{ff} adsorbate-adsorbate interaction parameter
ε_{mf} adsorbate-adsorbent interaction parameter
ϕ_i external field at site i
μ chemical potential
ρ_i local density in site i
σ characteristic length-scale in Lennard-Jones potential
Ω Grand potential

Acknowledgements SPR and PIC thank the EPSRC for financial support (under grant No. EP/D503906/1).

References

Barrett, E.P., Joyner, L.G., Halenda, P.H.: The determination of pore volume and area distributions in porous substances-I. Computations from nitrogen isotherms. J. Am. Chem. Soc. **73**, 373–380 (1951)

Cohan, L.H.: Sorption hysteresis and the vapor pressure of concave surfaces. J. Am. Chem. Soc. **60**, 433 (1938)

De Boer, J.H.: The shapes of capillaries. In: Everett, D.H., Stone, F.S. (eds.) The Structure and Properties of Porous Solids, pp. 68–94. Butterworths, London (1958)

Elias-Kohav, T., Sheintuch, M., Avnir, D.: Steady-state diffusion and reaction in catalytic fractal porous media, Chem. Eng. Sci. **46**, 2787–2798 (1991)

Esparza, J.M., Ojeda, M.L., Campero, A., Dominguez, A., Kornhauser, I., Rojas, F., Vidales, A.M., López, R.H., Zgrablich, G.: N_2 sorption scanning behaviour of SBA-15 porous substrates, Colloids Surf. A: Physicochem. Eng. Asp. **241**, 35–45 (2004)

Gregg, S.J., Sing, K.S.W.: Adsorption, Surface Area and Porosity. Academic Press, London (1982)

Hollewand, M.P., Gladden, L.F.: Transport heterogeneity in porous pellets-II. NMR imaging studies under transient and steady-state conditions. Chem. Eng. Sci. **50**, 309–326 (1995)

Kierlik, E., Monson, P.A., Rosinberg, M.L., Tarjus, G.: Adsorption hysteresis and capillary condensation in disordered porous solids: a density functional study. J. Phys.: Condens. Mater. **14**, 9295–9315 (2002)

Libby, B., Monson, P.A.: Adsorption/desorption hysteresis in ink-bottle pores: a density functional theory and Monte Carlo simulation study. Langmuir **20**, 4289–4294 (2004)

Morishige, K., Nakamura, Y.: Nature of adsorption and desorption branches in cylindrical pores. Langmuir **20**, 4503–4506 (2004)

Morishige, K., Tarui, N.: Capillary condensation of nitrogen in ordered mesoporous silica with bicontinuous gyroid structure. J. Phys. Chem. C **111**, 280–285 (2007)

Morishige, K., Tateishi, N.: Adsorption hysteresis in ink-bottle pore. J. Chem. Phys. **119**, 2301–2306 (2003)

Neimark, A.V., Ravikovitch, P.I.: Capillary condensation in MMS and pore structure characterization. Microporous Mesoporous Mater. **44–45**, 697–707 (2001)

Rigby, S.P.: A unified model for the effects of surface heterogeneity on gas absorption and surface diffusion on silica surfaces. In: Fong, P.A. (ed.) Colloid and Surface Research Trends, pp. 147–167. Nova Science Publishers, New York (2007)

Rigby, S.P., Edler, K.J.: The influence of mercury contact angle, surface tension and retraction mechanism on the interpretation of mercury porosimetry data. J. Colloid Interface Sci. **250**, 175–190 (2002)

Rigby, S.P., Fletcher, R.S.: Experimental evidence for pore blocking as the mechanism for nitrogen sorption hysteresis in a mesoporous material. J. Phys. Chem. B **108**, 4690–4695 (2004)

Rigby, S.P., Barwick, D., Fletcher, R.S., Riley, S.N.: Interpreting mercury porosimetry data for catalyst supports using semi-empirical alternatives to the Washburn equation. Appl. Catal. A **238**, 303–318 (2003)

Rigby, S.P., Chigada, P.I., Perkins, E.L., Lowe, J., Edler, K.J.: Fundamental studies of gas sorption within mesopores situated amidst an inter-connected, irregular network. Adsorption (2008). doi:10.1007/s10450-007-9091-8

Rouquerol, F., Rouquerol, J., Sing, K.: Adsorption by Powders and Porous Solids: Principles, Methodology and Applications. Academic Press, London (1999)